BIOCHEMISTRY
including biophysical chemistry & molecular biology

Article

pubs.acs.org/biochemistry

Mechanistic and Spectroscopic Studies of Metallo-β-lactamase NDM-1

Hao Yang, Mahesh Aitha, Alyssa M. Hetrick, Timothy K. Richmond, David L. Tierney, and Michael W. Crowder*

Department of Chemistry and Biochemistry, 160 Hughes Hall, Miami University, Oxford, Ohio 45056, United States

Supporting Information

ABSTRACT: In an effort to biochemically characterize metallo-β-lactamase NDM-1, we cloned, overexpressed, purified, and characterized several maltose binding protein (MBP)−NDM-1 fusion proteins with different N-termini (full-length, Δ6, Δ21, and Δ36). All MBP−NDM-1 fusion proteins were soluble; however, only one, MBP−NDM-1Δ36, exhibited high activity and bound 2 equiv of Zn(II). Thrombin cleavage of this fusion protein resulted in the truncated NDM-1Δ36 variant, which exhibited a k_{cat} of 16 s^{-1} and a K_m of 1.1 μM when using nitrocefin as a substrate, bound 2 equiv of Zn(II), and was monomeric in solution. Extended X-ray absorption fine structure studies of the NDM-1Δ36 variant indicate the average metal binding site for Zn(II) in this variant consists of four N/O donors (two of which are histidines) and 0.5 sulfur donor per zinc, with a Zn−Zn distance of 3.38 Å. This metal binding site is very similar to those of other metallo-β-lactamases that belong to the B1 subclass. Pre-steady-state kinetic studies using nitrocefin and chromacef and the NDM-1Δ36 variant indicate that the enzyme utilizes a kinetic mechanism similar to that used by metallo-β-lactamases L1 and CcrA, in which a reactive nitrogen anion is stabilized and its protonation is rate-limiting. While they are very different in terms of amino acid sequence, these studies demonstrate that NDM-1 is structurally and mechanistically very similar to metallo-β-lactamase CcrA.

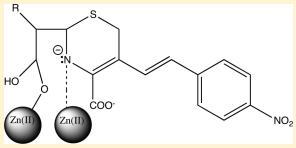

β-Lactam-containing antibiotics are relatively inexpensive but effective antimicrobial agents, which block bacterial cell wall synthesis resulting in cell lysis.[1] Since the introduction of β-lactam-containing antibiotics and other antibiotics in the clinic, bacteria have developed or acquired mechanisms to become resistant to those antibiotics.[2] The production of β-lactamases, which hydrolyze the C−N bond in the four-membered ring of the β-lactam, is the most common mechanism.[3] There have been more than 1000 distinct β-lactamases identified, and these enzymes have been categorized into classes A−D, based on their amino acid sequence homologies.[4] Class A, C, and D enzymes are collectively called serine-β-lactamases, and these enzymes use a common catalytic mechanism in which an active site serine nucleophilically attacks the β-lactam carbonyl, ultimately leading to a cleaved β-lactam ring. Class B enzymes are called metallo-β-lactamases (MBLs), and these enzymes utilize either 1 or 2 equiv of Zn(II) to catalyze the β-lactam hydrolysis reaction.[5] Class B MBLs have been further subgrouped into subclasses B1−B3, based on amino acid sequence homologies and Zn(II) content.[4−6] MBLs can hydrolyze almost all known β-lactam antibiotics, including carbapenems, which have been called one of the "last resort" antibiotics.[7]

To combat β-lactam resistance, new drugs targeting DNA synthesis or protein synthesis, instead of bacterial cell wall synthesis, were developed.[8] In addition, co-administration of β-lactam-containing antibiotics with β-lactamase inhibitors has proven to be an effective strategy for combatting antibiotic-resistant bacterial infections.[1] Unfortunately, β-lactamase inhibitors, such as clavulanate, sulbactam, and tazobactam, do not inhibit MBLs, and there are no clinically useful inhibitors of MBLs yet available.[9] MBLs have been isolated from clinical strains of *Stenotrophomonas maltophilia*, *Pseudomonas aeruginosa*, and *Acinetobacter baumannii*, which often cause nosocomial infections. However, most of the organisms that produce a MBL are not considered major pathogens, and the public health impact of MBL has been limited to date.[1,10]

The emergence of New Dehli metallo-β-lactamase (NDM-1) heralds a new era of antibiotic resistance because of the enzyme's ability to hydrolyze almost all known β-lactam-containing antibiotics and the rapid spread of the plasmid-encoded *NDM-1* gene.[11−16] The plasmid that harbors the NDM-1 gene is called *blaNDM-1* (also called *pNDM-1*), and this *blaNDM-1* plasmid often carries other resistance genes, such as genes conferring quinolone, sulfonamide, macrolide, and rifampicin resistance.[15] *blaNDM-1* was initially discovered in *Klebsiella* and *Escherichia coli* from a patient in Sweden who had surgery in India.[12] In the past two years, *blaNDM-1* has spread globally with unprecedented speed, having been detected on all continents except Central and South America and Antarctica.[15] *blaNDM-1* has even been isolated from bacteria in drinking water in India, indicating widespread environmental contamination.[17] Bacteria harboring NDM-1 are not susceptible to any common antibiotic, except colistin and tigecycline.[12] Considerable efforts have been made to structurally characterize NDM-1, and there are nine crystal structures of the enzyme available in the Protein Data Bank (PDB).[18−22] While there is some controversy about the number of Zn(II) ions bound in the physiologically relevant

Received: January 13, 2012
Revised: April 4, 2012
Published: April 6, 2012

   dx.doi.org/10.1021/bi300056y | *Biochemistry* 2012, 51, 3839−3847

form of NDM-1, several crystal structures showed two metal ions bound.[18,21,22] Zn_1 is coordinated by His120, His122, His189, and presumably a bridging hydroxide. Zn_2 is coordinated by His250, Asp124, Cys208, a terminally bound water, and the bridging hydroxide (Figure 1). The M−M distance has varied in the

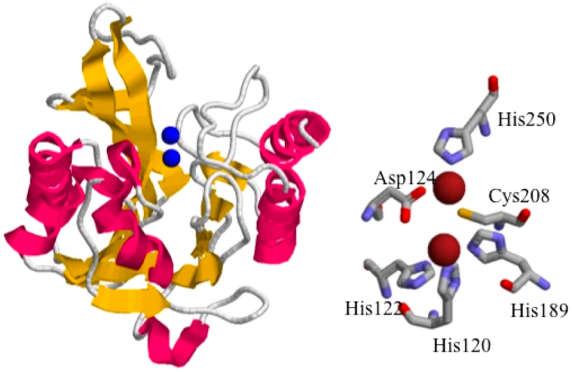

Figure 1. Structures of the subunit of NDM-1 (left) and the active site (right). This figure was rendered using Raswin version 2.7.3 and PDB entry 3Q6X.

different crystal structures (3.2−4.59 Å),[18,21−23] but the Zn−Zn distance appears to be <3.5 Å in most of the structures of uncomplexed, dinuclear Zn(II)-containing NDM-1. On the basis of the identity of active site residues, NDM-1 has been categorized into the MBL subclass B1; however, NDM-1 showed little amino acid sequence identity with other members of subclass B1. The most closely related MBL is VIM-2, and NDM-1 shares 32.4% sequence identity with this enzyme.[12] No mechanistic studies of NDM-1 have been reported.

Given the clinical significance of NDM-1, we describe herein biochemical and structural studies of NDM-1, including EXAFS and pre-steady-state kinetic studies. The goal was to elucidate the catalytic mechanism of NDM-1 using two chromogenic substrates, nitrocefin and chromacef (Figure 2), and to address

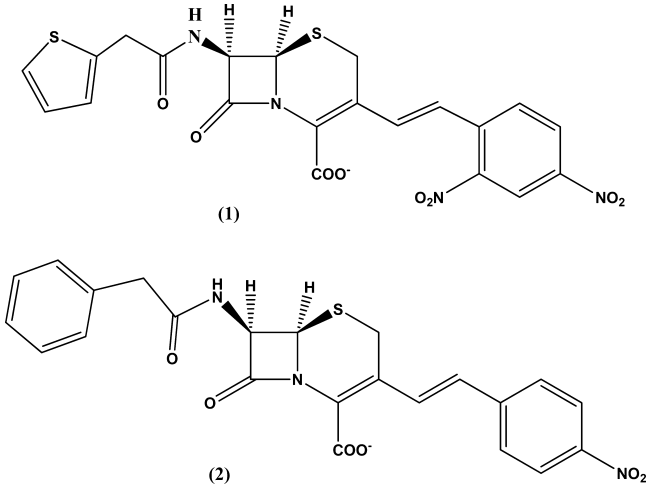

Figure 2. Structures of nitrocefin (**1**) and chromacef (**2**).

the conflicting data in the literature concerning the metal−metal distance in the enzyme. The ultimate goal of this project is to rationally design and prepare a clinically useful universal inhibitor of the MBLs. It is hoped that our identification of common mechanistic and structural aspects of the MBLs will reveal a viable inhibitor target.

EXPERIMENTAL PROCEDURES

Materials. *E. coli* strains DH5α and BL21(DE3) were purchased from Novagen (Madison, WI). The pET26b-full-length-NDM-1 plasmid was generously provided by J. Spencer (University of Bristol, Bristol, U.K.). The maltose binding protein (MBP)-containing vector, pIADL, was obtained from C. Walsh (Harvard Medical School, Boston, MA).[24] Digestion enzymes *Nde*I and *Hin*dIII were purchased from New England Biolabs. Primers for sequencing and amplifying different lengths of NDM-1 were purchased from Integrated DNA Technologies (Table 1). Isopropyl β-D-thiogalactoside (IPTG) was purchased from Anatrace (Maumee, OH). Bovine plasma thrombin was ordered from Sigma-Aldrich. Substrates nitrocefin (**1**) and chromacef (**2**) were purchased from Becton Dickinson and Sopharmia, respectively, and the solutions were made as previously reported.[25] All buffer solutions and growth media were made with Barnstead NANOpure, ultrapure water.

Construction of Overexpression Plasmids for Soluble MBP−NDM-1 Fusion Proteins. Expression vector pIADL, which encodes the maltose binding protein−VanX (MBP−VanX) fusion construct, was subjected to restriction digestion using *Nde*I and *Hin*dIII. The large (7.04 kb) piece was extracted by using a QIAquick kit (Qiagen, Valencia, CA). Primers with flanking with *Nde*I and *Hin*dIII restriction sites were designed to yield different lengths of NDM-1 (full-length NDM-1, NDM-1Δ6, NDM-1Δ21, and NDM-1Δ36) (Table 1). Polymerase chain reaction was used to produce the corresponding products, which were purified with a Qiagen gel extraction kit, digested with *Nde*I and *Hin*dIII, and purified again with a Qiagen gel extraction kit. The resulting NDM-1 genes were ligated into digested pIADL, generating overexpression plasmids for the MBP−NDM-1 fusion proteins. The ligation products were then transformed into chemically competent *E. coli* DH5α cells, and plasmids were purified using the Qiagen plasmid midi kit. The DNA sequences of the plasmids were verified by DNA sequencing.

Overexpression and Purification of MBP−NDM-1 Fusion Proteins. MBP−NDM-1 plasmids were transformed into *E. coli* BL21(DE3) cells, and the transformation mixtures were spread into lysogeny broth (LB) plates containing 25 μg/mL kanamycin. A single colony was transferred into 50 mL of LB containing 25 μg/mL kanamycin, and the culture was allowed to shake overnight at 37 °C. The overnight culture (10 mL) was transferred into 4 × 1 L of LB containing 25 μg/mL kanamycin. The resulting culture was grown at 37 °C with shaking at 220 rpm until an OD_{600} of 0.6−0.8 was reached. Protein production was induced by making the cultures 1 mM in IPTG. The cells were allowed to shake for 3 h at 37 °C, and then the cells were harvested by centrifugation for 10 min at 7000 rpm and 4 °C. The pellets were resuspended in 25 mL of 20 mM Tris (pH 7.6) containing 200 mM NaCl. The cells were lysed when the mixture was passed three times through a French press at a pressure of 1500 psi. The insoluble components were removed by centrifugation for 25 min at 15000 rpm. The supernatant was dialyzed versus 20 mM Tris (pH 7.6) containing 200 mM NaCl and 100 μM $ZnCl_2$ overnight. After centrifugation for an additional 25 min at 15000 rpm to remove the insoluble components, the cell lysate was loaded onto a pre-equilibrated amylose column (1.5 cm × 20 cm with a 26 mL bed volume). Proteins were eluted using a linear gradient from 20 mM Tris (pH 7.6) containing 200 mM NaCl and 100 μM $ZnCl_2$ to 20 mM Tris (pH 7.6) containing 200 mM NaCl and 10 mM maltose. Column fractions containing the MBP−NDM-1 fusion protein were

dx.doi.org/10.1021/bi300056y | *Biochemistry* 2012, 51, 3839−3847

Table 1. List of Primers (5′ → 3′) Used To Generate Different NDM-1 Variants

primer	sequence
full-length-NDM-1for	AAAAAACATATGGAATTGCCCAATATTATG
full-length-NDM-1rev	AAAAAAAAGCTTTCAGCGCAGCTTGTCGGC
NDM-1Δ6for	AAAAAACATATGCACCCGGTCGCGAAG
NDM-1Δ6rev	AAAAAAAAGCTTTCAGCGCAGCTTGTCGGC
NDM-1Δ21for	AAAAAACATATGCTGAGCGGGTGCATG
NDM-1Δ21rev	AAAAAAAAGCTTTCAGCGCAGCTTGTCGGC
NDM-1Δ36for	GGAATTCCATATGCAAATGGAAA
NDM-1Δ36rev	CCGCTCGAGTTAGCGCAGCTTGTCG

identified using a 15% sodium dodecyl sulfate−polyacrylamide gel electrophoresis (SDS−PAGE) gel, and fractions containing NDM-1 were collected and concentrated to 2−3 mL using an Amicon ultrafiltration concentrator equipped with a YM-10 membrane. The concentration of MBP−NDM-1 samples was estimated using the extinction coefficient of MBP (ε_{280} = 64500 M^{-1} cm^{-1})[26] added to the calculated extinction coefficients of the different truncated NDM-1 proteins. In-gel trypsin digestion followed by MALDI-TOF (matrix-assisted laser desorption ionization time-of-flight) mass spectrometry confirmed the presence of NDM-1.[27]

Thrombin Cleavage of MBP−NDM-1 Fusion Protein and NDM-1 Purification. To optimize the proteolysis conditions using thrombin, concentrated MBP−NDM-1 fusion protein was dialyzed overnight versus 2 L of 20 mM Tris-HCl (pH 8.4) containing 150 mM NaCl and 2.5 mM $CaCl_2$. To maximize the digestion efficiency and minimize the secondary digestions, bovine plasma thrombin was added at a ratio of 1.8 units of thrombin/mg of MBP−NDM-1 fusion protein, and the mixture was incubated at 15 °C for 2 h. The digestion reaction mixture was subjected to a Superdex 75 size exclusion column (1.5 cm × 40 cm with a 60 mL bed volume), using 30 mM Tris (pH 7.6) containing 200 mM NaCl as the running buffer. An amylose column (1.5 cm × 20 cm with a 26 mL bed volume) was used to further purify the NDM-1 samples after size exclusion. Fractions containing purified NDM-1 were identified using SDS−PAGE gels, and NDM-1 samples were collected and concentrated using an Amicon equipped with a YM-10 membrane. NDM-1 concentrations were determined by using the absorbances of the samples at 280 nm, the extinction coefficient (ε_{280} = 28500 M^{-1} cm^{-1}),[19] and Beer's law.

Metal Analyses. Inductively coupled plasma atomic emission spectroscopy (ICP-AES) was conducted to determine the metal content of MBP−NDM-1 and NDM-1 samples. Generally, the protein samples were diluted to 1 μM with Chelex-treated buffer [50 mM HEPES (pH 7.6)]. Standard calibration curves with correlation coefficients of >0.9999 were generated using serial dilutions of Fisher metal standards (Zn, Co, Cu, Fe, Mn, and Ni). The emission wavelengths used were 213.856 nm (Zn), 238.892 nm (Co), 324.754 nm (Cu), 259.940 nm (Fe), 257.610 nm (Mn), and 231.604 nm (Ni) to ensure the lowest detection limits possible.

Steady-State Kinetics. Steady-state kinetic studies were performed on a Hewlett-Packard 5480A UV−vis spectrophotometer at 22 °C. The hydrolysis of nitrocefin by MBP−NDM-1 and NDM-1 samples was monitored by detecting the formation of product at 485 nm, and absorbance data were converted into concentration data using a previously published extinction coefficient (Δε = 17420 M^{-1} cm^{-1}).[25] The hydrolysis of chromacef by NDM-1Δ36 was monitored by product formation, using a Δε of 18600 M^{-1} cm^{-1} (available on Sopharmia's website). The buffer used in kinetic studies consisted of 30 mM Tris (pH 7.6) and 200 mM NaCl. Substrate concentrations varied from 1 to 100 μM. The initial rate of product formation versus substrate was curve fit to the Michaelis−Menten equation using Igor-Pro to determine the steady-state kinetic constants K_m and k_{cat}.

EXAFS Spectroscopy. Samples for EXAFS spectroscopy (approximately 1 mM in protein) were prepared with 20% (v/v) glycerol as a glassing agent. EXAFS samples were loaded in Lucite cuvettes with 6 μm polypropylene windows and frozen rapidly in liquid nitrogen. X-ray absorption spectra were recorded at the National Synchrotron Light Source (NSLS), beamline X3B, with a Si(111) double-crystal monochromator; harmonic rejection was accomplished using a Ni focusing mirror. Fluorescence excitation spectra for all samples were measured with a 31-element solid-state Ge detector array. Samples were held at approximately 15 K in a Displex cryostat. EXAFS data collection and reduction were performed according to published procedures.[28] Data were measured in duplicate, four scans each on two samples from independent purifications; fits to the two data sets were equivalent. As both data sets gave similar results, the data were averaged using EXAFSPAK (EXAFSPAK is available free of charge from http://www-ssrl.slac.stanford.edu/~george/exafspak/exafs.htm); the experimental spectra presented here are the averaged data sets (eight scans per sample). The data were converted from energy to k space using the equation $k = \{[(2m_e)/\hbar^2](E - E_0)\}^{1/2}$ with an E_0 of 9680 eV.

Fourier-filtered EXAFS data were fit using the nonlinear least-squares engine of IFEFFIT, which is distributed with SixPack (SixPack is available free of charge from http://www.sssrl.slac.stanfrd.edu/_swebb/index.html; IFEFFIT is open source software available from http://www.cars9.uchicago.edu/ifeffit). Fourier-filtered EXAFS data were fit utilizing theoretical amplitude and phase functions calculated with FEFF version 8.00.[29] The zinc−nitrogen and zinc−sulfur scale factors and the threshold energy, ΔE_0, were calibrated to the experimental spectra for tetrakis-1-methylimidazole zinc(II) perchlorate, $Zn(MeIm)_4$[30] and $[N(Me)_4]_2[Zn(SPh)_4]$, and held fixed at 0.78 (Zn−N S_c), 0.85 (Zn−S S_c), and −21 eV (ΔE_0) in all subsequent fits to the data for NDM-1, unless otherwise noted. First-shell fits were then obtained for all reasonable coordination numbers, including mixed nitrogen/oxygen ligation, while the absorber−scatterer distance, R_{as}, and the Debye−Waller factor, σ_{as}^2, were allowed to vary. The best fits are presented in the Supporting Information. Multiple scattering contributions from histidine ligands were fit according to published procedures.[28] Metal−metal (zinc−zinc) scattering was modeled with reference to the experimental EXAFS of $Zn_2(salpn)_2$.[28]

Dynamic Light Scattering. Dynamic light scattering studies were conducted using a Zetasizer Nano (Malvern Instruments, Inc.). The samples were diluted to 10 μM using

dx.doi.org/10.1021/bi300056y | Biochemistry 2012, 51, 3839−3847

30 mM Tris (pH 7.6) containing 200 mM NaCl. The experiment was conducted at 25 °C. The protein samples were filtered through a 100 nm membrane before light scattering measurements were conducted. Three measurements were obtained for each sample. The average hydrodynamic size distribution of NDM-1Δ36 was determined with Zetasize software.

Pre-Steady-State Kinetics. To study the pre-steady-state kinetics of NDM-1, we conducted stopped-flow UV−vis studies on an Applied Photophysics SX 20 stopped-flow spectrophotometer equipped with a photodiode array detector and thermostated at 22 °C. The buffer used in these studies was Chelex-treated 30 mM Tris (pH 7.6) containing 200 mM NaCl. Nonlinear reaction parameters at all measured wavelengths were simultaneously fit with ProK kinetic software based on the proposed reaction mechanism in Scheme 1. The

Scheme 1. Kinetic Mechanism Used To Fit Pre-Steady-State Kinetic Data

$$E + S \underset{k_{-1}}{\overset{k_1}{\rightleftharpoons}} ES \underset{k_{-2}}{\overset{k_2}{\rightleftharpoons}} EI \xrightarrow{k_3} EP \underset{k_{-4}}{\overset{k_4}{\rightleftharpoons}} E+P$$

best-fit parameter sets were then used in KintekSim to simulate progress curves. The following molar extinction coefficients of nitrocefin were used: substrate ε_{390} = 11500 M^{-1} cm^{-1}, product ε_{485} = 17420 M^{-1} cm^{-1}, and intermediate ε_{665} = 32000 M^{-1} cm^{-1}.[31] The following molar extinction coefficients of chromacef were used: substrate ε_{378} = 22200 M^{-1} cm^{-1}, product ε_{442} = 18600 M^{-1} cm^{-1}, and intermediate ε_{575} = 22000 ± 2000 M^{-1} cm^{-1}. The extinction coefficient of the intermediate was determined by global analysis of the data[32] and by calculating the concentration of the intermediate at several time points.[31] The theoretical K_m and k_{cat} values were determined using the reaction mechanism in Scheme 1 and the King−Altman method,[33] assuming that k_3 is the rate-limiting step.

Principal component analysis (PCA) of the pre-steady-state kinetic data was conducted using Simca P+, starting with the spectra of substrate at time zero and the product at a time equal to 2 s. The PCA data were used to construct a physically real absorption spectrum of intermediate versus time. The corresponding PCA plots were fit using the ProK global analysis software and KintekSim, as described above. The extinction coefficient of the chromacef intermediate was determined to be 22000 M^{-1} cm^{-1}.

RESULTS

Overexpression, Purification, and Characterization of NDM-1 and MBP−NDM-1 Fusion Proteins. Initially, the full-length NDM-1 gene was ligated into pET26b, and this plasmid was transformed into *E. coli* BL21(DE3) cells. The resulting overexpressed NDM-1 was processed into inclusion bodies. Considering that the N-terminus might influence the Zn(II) binding affinity and catalytic activity of NDM-1,[23] we designed four recombinant constructs with fusion protein MBP, which is a chaperone protein and has been shown to improve protein folding and solubility.[26] MBP−full-length NDM-1, -Δ6, and -Δ21 and MBP−NDM-1Δ36 (first 6, 21, and 36 amino acids removed, respectively) fusion proteins were overexpressed and purified using amylose column chromatography. The MBP was removed from the fusion proteins by digestion with thrombin and by using size exclusion chromatography. The resulting NDM-1 samples were shown to be 95% pure by SDS−PAGE. NDM-1 was further purified (99%) by subjecting the protein samples to a second amylose column. Metal analyses showed that MBP−NDM-1Δ36, NDM-1Δ36, MBP−NDM-1Δ21, and unfused NDM-1 bind 2 equiv of Zn(II) (Table 2). However, NDM-1Δ21 binds only 1 equiv of Zn(II), even after incubation with excess Zn(II) followed by dialysis. Steady-state kinetic studies were conducted on the MBP fusion and unfused NDM-1 samples (Table 2) using nitrocefin as a substrate. NDM-1Δ21 and MBP−full-length NDM-1, -Δ6, and -Δ21 exhibited k_{cat} values of ∼1−2 s^{-1} and K_m values of ∼3 μM. NDM-1Δ36 and MBP−NDM-1Δ36 exhibited k_{cat} values of >15 s^{-1} and K_m values of 1.1 and 21.1 μM, respectively. Given these results, we used NDM-1Δ36 in all subsequent studies.

X-ray Absorption Spectroscopy. In an effort to show that recombinant NDM-1Δ36 is structurally similar to the NDM-1 previously reported, EXAFS data were obtained for the unfused enzyme. Fourier-transformed Zn K-edge EXAFS data for NDM-1Δ36 are shown in Figure 3. Detailed EXAFS curve-fitting results are presented in Table S1 of the Supporting Information. The data are best fit with a first shell (0.5−2.3 Å) of four nitrogen/oxygen donors at 2.01 Å and 0.5 S donor per Zn(II). Fit residuals improved dramatically upon inclusion of the sulfur contribution (Figure S1 and Table S1 of the Supporting Information). Multiple scattering analysis indicates an average of 2.0 ± 0.5 imidazole ligands per Zn(II) (fit S1-3, Figure S1 of the Supporting Information). Inclusion of a metal−metal scattering pathway at 3.38 Å improved the fit to the data by 37% (compare fit S1-3 to fit S1-4 in Figure S1 of the Supporting Information). Together, these data are consistent with a metal binding site in NDM-1Δ36 that coincides with a fully loaded B1MBL, with one Zn(II) coordinated by three histidines (in the Zn_1 or 3H site) and solvent, and the other Zn(II) coordinated by a single histidine (to give an average of two per Zn), and three low-Z donors, most likely oxygens from water and/or carboxylates, and a metal−metal separation of ∼3.4 Å,[34−39] very similar to that reported in previous crystallographic studies.[22]

Dynamic Light Scattering. To determine the oligomeric state of NDM-1Δ36, dynamic light scattering studies were performed. L1 was chosen as the control, which has been demonstrated to exist in a tetrameric state. The dimer and monomer controls of full-length NDM-1 were reported by Guo et al.[22] The radii of NDM-1Δ36 and L1 were 2.619 and

Table 2. Steady-State Kinetic Constants and Metal Contents of NDM-1 Samples

enzyme	k_{cat} (s^{-1})	K_m (μM)	k_{cat}/K_m (s^{-1} μM^{-1})	Zn(II) content (equiv)
MBP−full-length NDM-1	1.1 ± 0.1	2.0 ± 0.4	0.56	2.0 ± 0.1
MBP−NDM-1Δ6	1.4 ± 0.1	2.6 ± 0.2	0.51	2.1 ± 0.1
MBP−NDM-1Δ21	1.6 ± 0.1	3.0 ± 0.5	0.53	2.2 ± 0.1
NDM-1Δ21	2.6 ± 0.1	3.7 ± 0.5	0.69	1.0 ± 0.1
MBP−NDM-1Δ36	10.1 ± 0.1	3.2 ± 0.4	3.19	2.0 ± 0.1
NDM-1Δ36	16.1 ± 0.1	1.1 ± 0.1	14.8	2.0 ± 0.1

dx.doi.org/10.1021/bi300056y | *Biochemistry* 2012, 51, 3839−3847

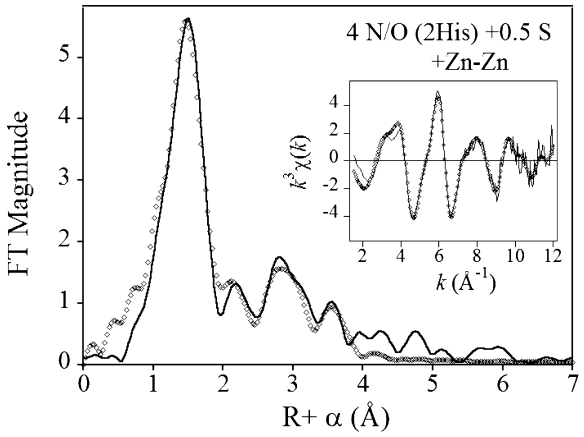

Figure 3. Fourier-transformed EXAFS of NDM-1Δ36 (—) and best fit (◇), including 0.5 S and 4 N/O donors, two of which are His ligands, per zinc and a distant Zn−Zn interaction. The inset shows a corresponding fit in k space. Detailed fitting results are presented in Figure S1 and Table S1 of the Supporting Information (fit S1-5).

4.739 nm, respectively, corresponding to masses of 24 and 108 kDa, respectively. These data are consistent with NDM-1Δ36 being a monomer in solution, in agreement with previous results.[22,23,40]

Mechanistic Studies. To investigate the reaction mechanism of NDM-1Δ36, we conducted stopped-flow kinetic studies using nitrocefin as the substrate. The reaction of 50 μM NDM-1Δ36 with 50 μM nitrocefin was monitored over a 500 ms time period (Figure 4A) using a stopped-flow mixer and diode-array detection. The spectra showed three prominent peaks (390, 485, and 665 nm). The peak at 390 nm is due to the absorbance of nitrocefin, and the peak at 485 nm is due to the absorbance of hydrolyzed nitrocefin.[31,32,41,42] The peak at 665 nm, the intensity of which increased during the first 30 ms of the reaction and decreased during subsequent times, is assigned to a ring-opened, nitrogen anionic form of hydrolyzed nitrocefin.[31,32,41,42] The absorbance data at 390, 485, and 665 nm in Figure 4A were converted into concentrations of the species and plotted versus time (Figure 4B).

To obtain the minimum kinetic reaction mechanism, stopped-flow spectra were analyzed using ProK global analysis software, using a Michaelis−Menten mechanism with a single intermediate (Scheme 1). ProK global analysis of the data resulted in rate constants that are listed in Table 3. We assumed diffusion control rates for substrate and product binding (k_1 and k_{-4}, respectively). Using the ProK global analysis rate constants, the initial concentrations of enzyme and substrate, and the Michaelis−Menten mechanism with a single intermediate, KintekSim was used to generate simulated progress curves. These simulated progress curves nicely overlay the experimental data (Figure 4B), except in the early time points of the substrate decay curve. The "dip" in substrate concentration data versus times has been observed many times in the past and has been attributed to overlapping absorbances of substrate and product/intermediate.[31,36,43−45] The shapes of the theoretical progress curves were greatly influenced by the values of k_2, k_{-2}, and k_3 and not greatly affected by the other microscopic rate constants. Because there were no discrete isosbestic points in the absorbance spectra (Figure 4A), we tested other mechanisms with additional intermediates; the use of these mechanisms did not result in improved fits. The King−Altman method was used to derive the expressions for theoretical k_{cat} and K_m values using the

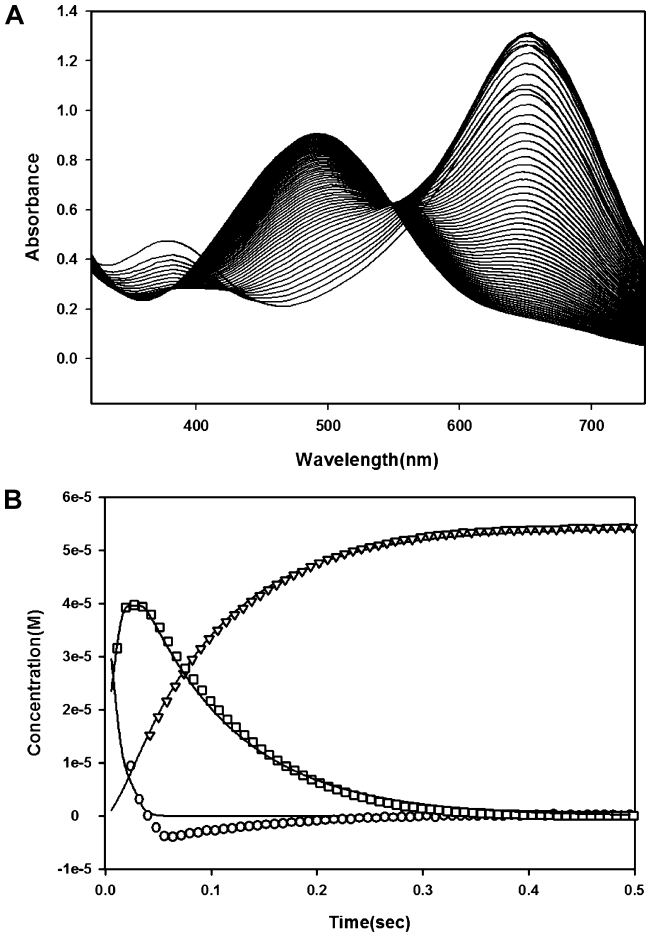

Figure 4. (A) Spectral changes during NDM-1Δ36-catalyzed hydrolysis of nitrocefin at pH 7.6 and 22 °C. The enzyme and substrate concentrations were 50 μM. The first spectrum was taken after a 2 ms mixing time, and the remaining spectra were collected every 2 ms. The reaction was complete in 50 ms. (B) Time course of the reaction of 50 μM NDM-1Δ36 with 50 μM nitrocefin at pH 7.6 and 22 °C. The absorbance values taken from panel A were converted to concentration values of substrate (○), product (◇), and intermediate (□), as described in the text. The lines are simulated progress curves (using KintekSim) using the global fit rates (Table 4) and the reaction mechanism in Scheme 1.

mechanism in Scheme 1 $\{k_{cat} = (k_2k_3)/(k_2 + k_{-2} + k_3)$; $K_m = (k_2 + k_{-1})(k_{-2} + k_3)/[k_1(k_2 + k_{-2} + k_3)]\}$. The rate constants in Table 3

Table 3. Results of Global Fitting Analyses of Stopped-Flow Kinetics of Nitrocefin Hydrolysis by NDM-1Δ36

constant	ProK global analysis[a]	KintekSim
k_1 (M^{-1} s^{-1})	1×10^8	1×10^8
k_{-1} (s^{-1})	3200 ± 700	3200 ± 700
k_2 (s^{-1})	150 ± 30	170 ± 10
k_{-2} (s^{-1})	<10	<4
k_3 (s^{-1})	13 ± 1	12 ± 1
k_4 (s^{-1})	4000 ± 1000	4600 ± 1400
k_{-4} (M^{-1} s^{-1})	1×10^8	1×10^8

[a]Data were fit with Applied Photophysics PC ProK global analysis software using the mechanism in Scheme 1.

were used to calculate the theoretical values of k_{cat} (11 s^{-1}) and K_m (2.6 μM), which are similar to experimental values (k_{cat} = 16.1 s^{-1}, and K_m = 1.1 μM).

dx.doi.org/10.1021/bi300056y | *Biochemistry* 2012, 51, 3839−3847

Because the pre-steady-state kinetic data did not exhibit discrete isosbestic points (Figure 4A), we also performed PCA analysis on the pre-steady-state kinetic data. The dip in the progress curves generated from the original data (Figure 4B) is no longer present in the progress curves generated from the PCA-analyzed data (Figure S2 of the Supporting Information), which confirms that the dip is due to overlapping absorbances of substrate and product/intermediate. The resulting PCA data were analyzed using ProK global analysis and KintekSim. The resulting microscopic rate constants and theoretical k_{cat} and K_m values were almost identical to those determined not using the PCA analysis (Figures S2 and S3 and Tables S2 and S3 of the Supporting Information).

To further test this mechanism, we conducted pre-steady-state kinetic studies using chromacef (Figure 2) as the substrate. The stopped-flow absorbance spectra are shown in Figure 5A. The three absorbance bands at 378, 442, and 575 nm correspond to substrate decay, product formation, and intermediate formation and decay, respectively. ProK global kinetic and KintekSim analyses, using the same reaction mechanism and assumptions that were used for nitrocefin (Scheme 1), were used to evaluate the data (Table 4 and Figure 5B). As with the nitrocefin data, there is a dip in the substrate concentration versus time plot (Figure 5B), and we attribute this dip to overlapping absorbances of substrate and product/intermediate.[31,36,43−45] King−Altman equations predict theoretical k_{cat} and K_m values of 13 ± 1 s^{-1} and 5.3 ± 0.5 μM, respectively, which are in excellent agreement with experimentally determined k_{cat} and K_m values of 10.8 s^{-1} and 8.3 μM, respectively. As with the nitrocefin data, PCA analysis (followed by global and KintekSim analysis) of the pre-steady-state kinetic data yielded microscopic rate constants that were nearly identical to those data not treated with PCA (Figure S3 and Table S3 of the Supporting Information). As with the nitrocefin data, the dip in the progress curve corresponding to chromacef decay is absent in the progress curve of PCA-analyzed data, demonstrating that the dip is due to overlapping absorbances of substrate with product/intermediate (Figure S3 of the Supporting Information).

DISCUSSION

First isolated from *Klebsiella pneumoniae* and *E. coli*, NDM-1 has spread to a number of other organisms and has been found across the globe except in Central and South America.[12,17] The overexpression and purification of recombinant NDM-1 has been reported by several groups,[18−23,40,46] and several crystal structures of unbound and inhibitor/product-bound variants of NDM-1 have been reported.[18−22] Steady-state kinetic studies of NDM-1 have revealed that the enzyme efficiently hydrolyzes all β-lactam-containing antibiotics except monobactams.[12,23] Nonetheless, there are significantly different values for the steady-state kinetic constants of NDM-1 reported by different groups, and there does appear to be some controversy about the number of Zn(II) ions bound by the purified enzyme and to the quaternary structure of the enzyme (monomer vs dimer).[18−22]

One of the challenges in studying NDM-1 has been not knowing the N-terminus of the soluble enzyme. Several N-terminal sequencing algorithms predicted N-termini of Ala19 and Gly29 and predicted that Cys26 is lipid-modified.[20,21,47] Crystal structures have been reported for NDM-1 variants with an N-terminal Met27 or Gly47 residue.[20,22] Recently, Thomas et al. demonstrated that *E. coli* processes NDM-1 containing an N-terminus of Ala16, Ala18, Ala19, or Gly36, with the analogue having the Gly36 terminus as the major form.[23]

We initially overexpressed full-length NDM-1 using a pET26b-based expression system, and we discovered that the

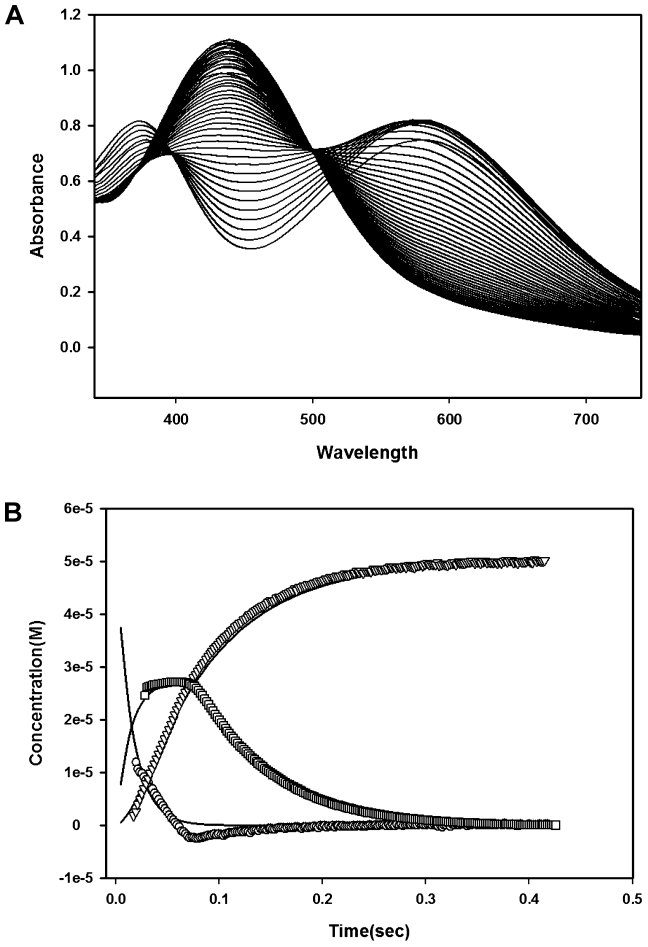

Figure 5. (A) Spectral changes during NDM-1Δ36-catalyzed hydrolysis of chromacef at pH 7.6 and 22 °C. The enzyme and substrate concentrations were 50 μM. The first spectrum was taken after a 2 ms mixing time, and the remaining spectra were collected every 2 ms. The reaction was complete in 50 ms. (B) Time course of the reaction of 50 μM NDM-1Δ36 with 50 μM chromacef at pH 7.6 and 22 °C. The absorbance values taken from panel A were converted to concentration values of substrate (○), product (▽), and intermediate (□), as described in the text. The lines are simulated progress curves (using KintekSim) using the global fit rates (Table 4) and the reaction mechanism in Scheme 1.

Table 4. Results of Global Fitting Analyses of Stopped-Flow Kinetics of Chromacef Hydrolysis by NDM-1Δ36

constant	ProK global analysis[a]	KintekSim
k_1 (M^{-1} s^{-1})	1 × 10^8	1 × 10^8
k_{-1} (s^{-1})	3200 ± 500	3200 ± 800
k_2 (s^{-1})	165 ± 10	180 ± 10
k_{-2} (s^{-1})	16 ± 2	16 ± 2
k_3 (s^{-1})	20 ± 1	16 ± 4
k_4 (s^{-1})	4000 ± 2000	4600 ± 1400
k_{-4} (M^{-1} s^{-1})	1 × 10^8	1 × 10^8

[a]Data were fit with Applied Photophysics PC ProK global analysis software using the mechanism in Scheme 1. Constants k_1 and k_{-4} as diffusion-controlled limits were fixed during the fitting using ProK global analysis.

dx.doi.org/10.1021/bi300056y | *Biochemistry* 2012, 51, 3839−3847

resulting overexpressed protein was insoluble, which was previously reported by Kim et al.[19] In an effort to solubilize the enzyme, we subcloned the full-length NDM-1 gene into a plasmid that generated a MBP−NDM-1 fusion protein. Although it was soluble and contained 2 equiv of Zn(II), the resulting MBP−NDM-1 fusion protein exhibited a low k_{cat}, as compared to those of some of the previously reported variants of NDM-1.[23] Therefore, several different MBP−NDM-1 fusion proteins, with truncated NDM-1 genes (MBP−NDM-1Δ6, MBP−NDM-1Δ21, and MBP−NDM-1Δ36), were generated and subjected to overexpression, purification, and characterization. Several steady-state kinetic studies have been reported on NDM-1 when using a wide variety of β-lactam-containing compounds as substrates,[19,23,46,48] with K_m values for full-length NDM-1 and NDM-1Δ29 ranging from 16 to 94 μM and k_{cat} values ranging from 11 to 20 s^{-1}. In contrast, NDM-1Δ36 and NDM-1Δ38 variants exhibited K_m values ranging from 45 to 310 μM and k_{cat} values ranging from 138 to 720 s^{-1} when using the same substrates.[23]

In previous studies using nitrocefin as a substrate, K_m and k_{cat} values for truncated NDM-1 variants have ranged from 1 to 3 μM and from 12 to 15 s^{-1}, respectively.[19,23] In our hands, full-length MBP−NDM-1, MBP−NDM-1Δ7, MBP−NDM-1Δ22, and NDM-1Δ22 exhibited very low catalytic activities toward nitrocefin with k_{cat} values of ∼2 s^{-1} (Table 2). Consistent with previous studies of truncated NDM-1 variants,[19,23] MBP−NDM-1Δ36 and NDM-1Δ36 showed the highest catalytic activity toward nitrocefin with a k_{cat} value of 15 s^{-1} (Table 2).

Previous studies of NDM-1 have demonstrated the NDM-1 can be isolated as an apoenzyme or an enzyme containing 0.2−2.0 equiv of Zn(II), depending on isolation conditions and whether there is a N-terminal signal peptide on the enzyme.[18,19,21−23,49] In this work, all NDM-1 samples bound 2 equiv of Zn(II), except NDM-1Δ21, which bound only 1 equiv of Zn(II). We speculate this may be due to oxidation of the metal binding cysteine.[23,50] Dynamic light scattering was performed on NDM-1Δ36 to determine the enzyme's oligomeric state. The radius of NDM-1Δ36 is close to that of the NDM-1 monomer control and much smaller than that of the dimer control published by Rao,[22] indicating that NDM-1Δ36 is monomeric. This result is consistent with previous light scattering, crystallographic, analytical centrifugation, and size-exclusion chromatographic results[22,23,48] but in contrast to previous studies that suggested that full-length NDM-1 is dimeric.[20] Given our studies and previous reports, it is clear that the N-terminus of NDM-1 affects the catalytic activity, oligomerization, and possibly metal content of the enzyme.

In our hands, NDM-1Δ36 exhibited the greatest catalytic activity, and two Zn(II) ions bound to this variant. We decided to use this variant in all subsequent studies. EXAFS of this variant was best fit with an average Zn(II) coordination sphere that matches nicely with those of other B1 MBLs, with an average ligand environment of two His, 0.5 Cys, and 2.5 other low-Z ligands, presumably water and or carboxylate oxygen. The metal−metal distance is 3.38 Å for NDM-1Δ36, which is between the crystallographically determined distance of 3.2 Å[22] and the QM/MM modeling-determined distance of 3.58 Å[23] but significantly shorter than M−M distances reported for the NDM-1−product complex (4.59 Å)[21] and the Zn−Cd distance (3.64 Å).[18] While there are conflicting values for the M−M distance in NDM-1 from crystallographic studies, the EXAFS data for NDM-1Δ36 are consistent with previous data for other metallo-β-lactamases,[34−39] and these data nicely show how this truncated NDM-1 variant fits into the B1 subclass and that this variant can be used for future rapid-freeze-quench spectroscopic studies.

To probe the catalytic mechanism of NDM-1Δ36, pre-steady-state kinetic studies were performed using nitrocefin as the substrate, as previously reported for L1,[31,43,44] CcrA,[41,42] GOB,[51] ImiS,[52] Bla2,[37] BcII,[53,54] and IMP-1.[36] In studies of L1 and CcrA, a ring-opened, nitrogen anion of nitrocefin was detected at 665 nm using diode array spectroscopic studies. A similar intermediate was not detected in studies of GOB, Bla2, BcII, ImiS, or IMP-1. In diode array spectroscopic studies of NDM-1Δ36, an intense, transient peak at 665 nm was observed (Figure 4A), demonstrating that the metal binding site in NDM-1 can stabilize the nitrocefin-derived reaction intermediate. Surprisingly, the diode array spectra of the NDM-1-catalyzed hydrolysis of nitrocefin did not reveal two discrete isosbestic points, suggesting that NDM-1 may catalyze a reaction with more than one intermediate. Nonetheless, we used kinetic simulations and ProK global analyses to fit the diode array data to the same minimal kinetic mechanism that was used to fit data on CcrA and L1 (Scheme 1) as well as to kinetic mechanisms with additional intermediates. Our analyses demonstrated the diode array spectroscopic data on NDM-1 can be adequately fit using the mechanism in Scheme 1, and rate constants determined using the global analysis software can be used to calculate theoretical progress curves that overlay the experimental data (Figure 4B). As a second confirmation of the mechanism, we used the King−Altman method to derive theoretical expressions for k_{cat} and K_m, and the calculated k_{cat} and K_m values were almost identical to the experimentally determined steady-state kinetic constants. These lines of evidence support the idea that the minimal kinetic mechanism shown in Scheme 1 is the mechanism used by NDM-1 to catalyze the hydrolysis of nitrocefin.

To further test the kinetic mechanism of NDM-1, we probed the reaction of chromacef with the enzyme. Previously, it was hypothesized that the stabilization of the nitrocefin-derived intermediate was due to resonance stabilization of the nitrogen anion into the dinitro-substituted styryl group (Figure 2).[32,41,42] A new chromogenic substrate, chromacef, was recently introduced with a p-nitrostyryl substituent (Figure 2). Like studies with nitrocefin, diode array spectroscopic studies of the reaction of NDM-1 with chromacef resulted in three absorbances: a peak at 378 nm that corresponds to substrate, a peak at 442 nm that corresponds to hydrolyzed product, and a peak at 575 nm that corresponds to a reaction intermediate, similar to the nitrocefin-derived nitrogen anion. ProK global analyses were used to fit these data to the kinetic mechanism shown in Scheme 1, and KintekSim and King−Altman analyses were used to validate the mechanism. In reactions with nitrocefin and chromacef, the rate-limiting step is the breakdown of the intermediate, specifically the protonation of the putative ring-opened nitrogen anion. These studies demonstrate that the reactions of NDM-1, or other MBLs, with nitrocefin and chromacef can be probed in a similar way. These studies also suggest that NDM-1 has a geometrically organized metal binding site that is positioned to stabilize the nitrocefin- and chromacef-derived intermediates, as the sites in CcrA and L1 are. With BcII, a nitrocefin-based intermediate has not been observed[53] but an imipenem- and meropenem-based intermediate may be formed.[55] The remaining metallo-β-lactamases have yet to be shown to stabilize this intermediate, and this been attributed to subtle differences in the metal binding sites in the enzymes.[53]

dx.doi.org/10.1021/bi300056y | Biochemistry 2012, 51, 3839−3847

In conclusion, NDM-1Δ36 is an excellent variant of the enzyme for conducting future spectroscopic and mechanistic studies. While most similar to VIM-2 in terms of amino acid sequence,[56] the metal binding site and architecture are more similar to those of CcrA.[32,57] Mechanistically, NDM-1 is similar to L1 and CcrA. Nonetheless, the crystal structures of NDM-1 show subtle differences in the positions of loops and domains, and these structures may be important for substrate recognition and catalysis. Efforts are underway to further probe the reaction mechanism of NDM-1 and the role of these loops and domains in catalysis and binding.

■ ASSOCIATED CONTENT

Ⓢ Supporting Information

Additional EXAFS spectra and fitting data and progress curves and kinetic fitting data after absorbance data had been analyzed by PCA. This material is available free of charge via the Internet at http://pubs.acs.org.

■ AUTHOR INFORMATION

Corresponding Author

*E-mail: crowdemw@muohio.edu. Phone: (513) 529-7274. Fax: (513) 529-5715.

Funding

This work was supported by the National Institutes of Health (Grant GM093987 to M.W.C. and D.L.T.) and a Miami University/Volwiler Professorship (to M.W.C.).

Notes

The authors declare no competing financial interest.

■ ABBREVIATIONS

EXAFS, extended X-ray absorption fine structure; MBL, metallo-β-lactamase; MBP, maltose binding protein; NDM-1, New Delhi metallo-β-lactamase.

■ REFERENCES

(1) Drawz, S. M., and Bonomo, R. A. (2010) Three decades of β-lactamase inhibitors. *Clin. Microbiol. Rev. 23*, 160−201.

(2) Wright, G. D. (2011) Molecular mechanisms of antibiotic resistance. *Chem. Commun. 47*, 4055−4061.

(3) Fisher, J. F., Meroueh, S. O., and Mobashery, S. (2005) Bacterial resistance to β-lactam antibiotics: Compelling opportunism, compelling opportunity. *Chem. Rev. 105*, 395−424.

(4) Bush, K., and Jacoby, G. A. (2010) Updated functional classification of β-lactamases. *Antimicrob. Agents Chemother. 54*, 969−976.

(5) Crowder, M. W., Spencer, J., and Vila, A. J. (2006) Metallo-β-lactamases: Novel weaponry for antibiotic resistance in bacteria. *Acc. Chem. Res. 39*, 721−728.

(6) Bebrone, C. (2007) Metallo-β-lactamases (classification, activity, genetic organization, structure, zinc coordination) and their superfamily. *Biochem. Pharmacol. 74*, 1686−1701.

(7) Papp-Wallace, K. M., Endimiani, A., Taracila, M. A., and Bonomo, R. A. (2011) Carbapenems: Past, Present, and Future. *Antimicrob. Agents Chemother. 55*, 4943−4960.

(8) Livermore, D. M. (2011) Discovery research: The scientific challenge of finding new antibiotics. *J. Antimicrob. Chemother. 66*, 1941−1944.

(9) Perez-Llarena, F., and Bou, G. (2009) β-Lactamase Inhibitors: The story so far. *Curr. Med. Chem. 16*, 3740−3765.

(10) Walsh, T. R., Toleman, M. A., Poirel, L., and Nordmann, P. (2005) Metallo-β-lactamases: The quiet before the storm? *Clin. Microbiol. Rev. 18*, 306−325.

(11) Bonomo, R. A. (2011) New Delhi metallo-β-lactamase and multidrug resistance: A global SOS? *Clin. Infect. Dis. 52*, 485−487.

(12) Kumarasamy, K. K., Toleman, M. A., Walsh, T. R., Bagaria, J., Butt, F., Balakrishnan, R., Chaudhary, U., Doumith, M., Giske, C. G., Irfan, S., Krishnan, P., Kumar, A. V., Maharjan, S., Mushtaq, S., Noorie, T., Paterson, D. L., Pearson, A., Perry, C., Pike, R., Rao, B., Ray, U., Sarma, J. B., Sharma, M., Sheridan, E., Thirunarayan, M. A., Turton, J., Upadhyay, S., Warner, M., Welfare, W., Livermore, D. M., and Woodford, N. (2010) Emergence of a new antibiotic resistance mechanism in India, Pakistan, and the UK: A molecular, biological, and epidemiological study. *Lancet Infect. Dis. 10*, 597−602.

(13) Koh, T. H., Khoo, C. T., Wijaya, L., Leong, H. N., Lo, Y. L., Lim, L. C., and Koh, T. Y. (2010) Global spread of New Delhi metallo-β-lactamase 1. *Lancet Infect. Dis. 10*, 828.

(14) Rolain, J. M., Parola, P., and Cornaglia, G. (2010) New Delhi metallo-β-lactamase (NDM-1): Towards a new pandemia? *Clin. Microbiol. Infect. 16*, 1699−1701.

(15) Nordmann, P., Poirel, L., Walsh, T. R., and Livermore, D. M. (2011) The emerging NDM carbapenemases. *Trends Microbiol. 19*, 588−595.

(16) Lascols, C., Hackel, M., Marshall, S. H., Hujer, A. M., Bouchillon, S., Badal, R., Hoban, D., and Bonomo, R. A. (2011) Increasing prevalence and dissemination of NDM-1 metallo-β-lactamase in India: Data from the SMART study (2009). *J. Antimicrob. Chemother. 66*, 1992−1997.

(17) Walsh, T. R., Weeks, J., Livermore, D. M., and Toleman, M. A. (2011) Dissemination of NDM-1 positive bacteria in the New Delhi environment and its implications for human health: An environmental point prevalence study. *Lancet Infect. Dis. 11*, 355−362.

(18) Green, V. L., Verma, A., Owens, R. J., Phillips, S. E. V., and Carr, S. B. (2011) Structure of New Delhi metallo-β-lactamase 1 (NDM-1). *Acta Crystallogr. F67*, 1160−1164.

(19) Kim, Y., Tesar, C., Mire, J., Jedrzejczak, R., Binkowski, A., Babnigg, G., Sacchettini, J., and Joachimiak, A. (2011) Structure of apo- and monometalated forms of NDM-1: A highly potent carbapenem-hydrolyzing metallo-β-lactamase. *PLoS One 6*, e24621.

(20) King, D., and Strynadka, N. (2011) Crystal structure of New Delhi metallo-β-lactamase reveals molecular basis for antibiotic resistance. *Protein Sci. 20*, 1484−1491.

(21) Zhang, H., and Hao, Q. (2011) Crystal structure of NDM-1 reveals a common β-lactam hydrolysis mechanism. *FASEB J. 25*, 2574−2582.

(22) Guo, Y., Wang, J., Niu, G., Shui, W., Sun, Y., Zhou, H., Zhang, Y., Yang, C., Lou, Z., and Rao, Z. (2011) A structural view of the antibiotic degradation enzyme NDM-1 from a superbug. *Protein Cell 2*, 384−394.

(23) Thomas, P. W., Zheng, M., Wu, S., Guo, H., Liu, D., Xu, D., and Fast, W. (2011) Characterization of purified New Delhi metallo-β-lactamase-1. *Biochemistry 50*, 10102−10113.

(24) McCafferty, D. G., Lessard, I. A. D., and Walsh, C. T. (1997) Mutational Analysis of Potential Zinc-Binding Residues in the Active Site of the Enterococcal D-Ala-D-Ala Dipeptidase VanX. *Biochemistry 36*, 10498−10505.

(25) Crowder, M. W., Walsh, T. R., Banovic, L., Pettit, M., and Spencer, J. (1998) Overexpression, Purification, and Characterization of the Cloned Metallo-β-Lactamase L1 from *Stenotrophomonas maltophilia*. *Antimicrob. Agents Chemother. 42*, 921−926.

(26) Breece, R. M., Costello, A., Bennett, B., Sigdel, T. K., Matthews, M. L., Tierney, D. L., and Crowder, M. W. (2005) A five-coordinate metal center in Co(II)-substituted VanX. *J. Biol. Chem. 280*, 11074−11081.

(27) Sigdel, T. K., Cilliers, R., Gursahaney, P. R., and Crowder, M. W. (2004) Fractionation of soluble proteins in *Escherichia coli* using DEAE-, SP-, and phenyl sepharose chromatographies. *J. Biomol. Tech. 15*, 199−207.

(28) Thomas, P. W., Stone, E. M., Costello, A., Tierney, D. L., and Fast, W. (2005) The quorum-quenching lactonase from *Bacillus thuringiensis* is a metalloprotein. *Biochemistry 44*, 7559−7569.

(29) Ankudinov, A. L., Ravel, B., Rehr, J. J., and Conradson, S. D. (1998) Real-space multiple-scattering calculation and interpretation of X-ray-absorption near-edge structure. *Phys. Rev. B 58*, 7565−7576.
(30) McClure, C. P., Rusche, K. M., Pearlso, K., Jackman, J. E., Fierke, C. A., and Penner-Hahn, J. E. (2003) EXAFS studies of the zinc sites of UDP-(3-O-acyl)-N-acetylglucosamine deacetylase (LpxC). *J. Inorg. Biochem. 94*, 78−85.
(31) McManus-Munoz, S., and Crowder, M. W. (1999) Kinetic mechanism of metallo-β-lactamase L1 from *Stenotrophomonas maltophilia*. *Biochemistry 38*, 1547−1553.
(32) Wang, Z., Fast, W., and Benkovic, S. J. (1999) On the Mechanism of the Metallo-β-Lactamase from *Bacteroides fragilis*. *Biochemistry 38*, 10013−10023.
(33) Segel, I. H. (1993) *Enzyme Kinetics*, John Wiley and Sons, Inc., New York.
(34) Abriata, L. A., Gonzalez, L. J., Llarrull, L. I., Tomatis, P. E., Myers, W. K., Costello, A. L., Tierney, D. L., and Vila, A. J. (2008) Engineered mononuclear variants in *Bacillus cereus* metallo-β-lactamase BcII are inactive. *Biochemistry 47*, 8590−8599.
(35) Gonzalez, J. M., Medrano Martin, F. J., Costello, A. L., Tierney, D. L., and Vila, A. J. (2007) The Zn_2 position in metallo-β-lactamases is critical for activity: A study on chimeric metal sites on a conserved protein scaffold. *J. Mol. Biol. 373*, 1141−1156.
(36) Griffin, D. H., Richmond, T. K., Sanchez, C., Moller, A. J., Breece, R. M., Tierney, D. L., Bennett, B., and Crowder, M. W. (2011) Structural and kinetic studies on metallo-β-lactamase IMP-1. *Biochemistry 50*, 9125−9134.
(37) Hawk, M. J., Breece, R. M., Hajdin, C. E., Bender, K. M., Hu, Z., Costello, A. L., Bennett, B., Tierney, D. L., and Crowder, M. W. (2009) Differential binding of Co(II) and Zn(II) to metallo-β-lactamase Bla2 from *Bacillus anthracis*. *J. Am. Chem. Soc. 131*, 10753−10762.
(38) Periyannan, G., Costello, A. L., Tierney, D. L., Yang, K. W., Bennett, B., and Crowder, M. W. (2006) Sequential binding of cobalt(II) to metallo-β-lactamase CcrA. *Biochemistry 45*, 1313−1320.
(39) Campos-Bermudez, V. A., Gonzalez, J. M., Tierney, D. L., and Vila, A. J. (2010) Spectroscopic signature of a ubiquitous metal binding site in the metallo-β-lactamase superfamily. *J. Biol. Inorg. Chem. 15*, 1209−1218.
(40) Zheng, B., Tan, S., Gao, J., Han, H., Liu, J., Lu, G., Liu, D., Yi, Y., Zhu, B., and Gao, G. F. (2011) An unexpected similarity between antibiotic-resistant NDM-1 and β-lactamase II from *Erythrobacter litoralis*. *Protein Cell 2*, 250−258.
(41) Wang, Z., and Benkovic, S. J. (1998) Purification, Characterization, and Kinetic Studies of Soluble *Bacteroides fragilis* Metallo-β-Lactamase. *J. Biol. Chem. 273*, 22402−22408.
(42) Wang, Z., Fast, W., and Benkovic, S. J. (1998) Direct Observation of an Enzyme-Bound Intermediate in the Catalytic Cycle of the Metallo-β-Lactamase from *Bacteroides fragilis*. *J. Am. Chem. Soc. 120*, 10788.
(43) Garrity, J. D., Bennett, B., and Crowder, M. W. (2005) Direct evidence that reaction intermediate in metallo-β-lactamase is metal bound. *Biochemistry 44*, 1078−1087.
(44) Hu, Z., Periyannan, G., Bennett, B., and Crowder, M. W. (2008) Role of the Zn_1 and Zn_2 sites in metallo-β-lactamase L1. *J. Am. Chem. Soc. 130*, 14207−14216.
(45) Hu, Z., Spadafora, L. J., Hajdin, C. E., Bennett, B., and Crowder, M. W. (2009) Structure and mechanism of copper- and nickel-substituted analogues of metallo-β-lactamase L1. *Biochemistry 48*, 2981−2989.
(46) Liang, Z., Li, L., Wang, Y., Chen, L., Kong, X., Hong, Y., Lan, L., Zheng, M., Guang-Yang, C., Liu, H., Shen, X., Luo, C., Li, K. K., Chen, K., and Jiang, H. (2011) Molecular basis of NDM-1, a new antibiotic resistance determinant. *PLoS One 6*, e23606.
(47) Yong, D., Toleman, M. A., Giske, C. G., Cho, H. S., Sundman, K., Lee, K., and Walsh, T. R. (2009) Characterization of a new metallo-β-lactamase gene, bla(NDM-1), and a novel erythromycin esterase gene carried on a unique genetic structure in *Klebsiella pneumoniae* sequence type 14 from India. *Antimicrob. Agents Chemother. 53*, 5046−5054.
(48) Yong, D., Toleman, M. A., Giske, C. G., Cho, H. S., Sundman, K., Lee, K., and Walsh, T. R. (2009) Characterization of a new metallo-β-lactamase gene, blaNDM-1, and a novel erythromycin esterase gene carried on a unique genetic structure in *Klebsiella pneumoniae* sequence type 14 from India. *Antimicrob. Agents Chemother. 53*, 5046−5054.
(49) King, M. D., Blanton, T. N., and Korter, T. M. (2011) Revealing the true crystal structure of λ-phenylalanine using solid-state density functional theory. *Phys. Chem. Chem. Phys. 14*, 1113−1116.
(50) Crowder, M. W., Yang, K. W., Carenbauer, A. L., Periyannan, G., Seifert, M. A., Rude, N. E., and Walsh, T. R. (2001) The Problem of a Solvent Exposable Disulfide when Preparing Co(II)-Substituted Metallo-β-Lactamase L1 from *Stenotrophomonas maltophilia*. *J. Biol. Inorg. Chem. 6*, 91−99.
(51) Moran-Barrio, J., Gonzalez, J. M., Lisa, M. N., Costello, A. L., Dal Peraro, M., Carloni, P., Bennett, B., Tierney, D. L., Limansky, A. S., Viale, A. M., and Vila, A. J. (2007) The metallo-β-lactamase GOB is a mono-Zn(II) enzyme with a novel active site. *J. Biol. Chem. 282*, 18286−18293.
(52) Sharma, N. P., Hajdin, C., Chandrasekar, S., Bennett, B., Yang, K. W., and Crowder, M. W. (2006) Mechanistic studies on the mononuclear Zn(II)-containing metallo-β-lactamase ImiS from *Aeromonas sobria*. *Biochemistry 45*, 10729−10738.
(53) Rasia, R. M., and Vila, A. J. (2003) Mechanistic study of the hydrolysis of nitrocefin mediated by *B. cereus* metallo-β-lactamase. *ARKIVOC 3*, 507−516.
(54) Llarrull, L. I., Tioni, M. F., Kowalski, J., Bennett, B., and Vila, A. J. (2007) Evidence for a Dinuclear Active Site in the Metallo-β-lactamase BcII with Substoichiometric Co(II): A new model for metal uptake. *J. Biol. Chem. 282*, 30586−30595.
(55) Tioni, M. F., Llarrull, L. I., Poeylaut-Palena, A. A., Marti, M. A., Saggu, M., Periyannan, G. R., Mata, E. G., Bennett, B., Murgida, D. H., and Vila, A. J. (2008) Trapping and characterization of a reaction intermediate in carbapenem hydrolysis by *B. cereus* metallo-β-lactamase. *J. Am. Chem. Soc. 130*, 15852−15863.
(56) Mavroidi, A., Tsakris, A., Tzelepi, E., Pournaras, S., Loukova, V., and Tzouvelekis, L. S. (2000) Carbapenem-Hydrolysing VIM-2 Metallo-β-Lactamase in *Pseudomonas aeruginosa* from Greece. *J. Antimicrob. Chemother. 46*, 1041−1043.
(57) Concha, N. O., Rasmussen, B. A., Bush, K., and Herzberg, O. (1996) Crystal Structure of the Wide-Spectrum Binuclear Zinc β-Lactamase from *Bacteroides fragilis*. *Structure 4*, 823−836.